

# Multi-channel system for imaging laser accelerated proton beams

Contact | [james.green@stfc.ac.uk](mailto:james.green@stfc.ac.uk)

**J. S. Green, S. P. Blake, C. Brenner\*,  
F. H. Cameron, B. Costello,  
P. S. Foster\*\*, P. Gallegos\*,  
M. G. J. Henderson, D. R. Neville,  
P. P. Rajeev, M. J. V. Streeter and  
D.N. Neely\***

*Central Laser Facility, STFC, Rutherford  
Appleton Laboratory, HSIC, Didcot,  
Oxon OX11 0QX, UK*

**M. Borghesi, R. Prasad, K. E. Quinn,  
L. Romagnani, S. Ter-Avetisyan  
and M. Zepf**

*Department of Physics and Astronomy,  
Queens University Belfast, BT7 1NN, UK*

**D. C. Carroll, P. McKenna and  
O. Tresca**

*SUPA, Department of Physics, University  
of Strathclyde, Glasgow, G4 0NG, UK*

**N. Dover, Z. Najmudin, C. Palmer  
and J. Schreiber**

*Blackett Laboratory, Imperial College  
London, SW7 2BZ, UK*

*\*also at SUPA, Department of Physics,  
University of Strathclyde. Glasgow,  
G4 0NG, UK*

*\*\* also at Department of Physics and  
Astronomy, Queens University Belfast,  
BT7 1NN, UK*

## Introduction

The generation of multi-MeV proton beams from high-intensity, short-pulse laser interactions has remained a topic of significant experimental<sup>[1-3]</sup> and theoretical<sup>[4-8]</sup> interest over recent years. A number of key experiments performed over the past few years have sought not only to understand the nature of the acceleration mechanisms, but also to control and optimise proton beam production<sup>[9-11]</sup> in order to realize future applications, such as proton fast ignition<sup>[12,13]</sup> or medical treatments<sup>[14]</sup>.

Radiochromic film (RCF)<sup>[15]</sup> stacks are often employed when spatial and spectral information of a proton beam is required. These dosimetry films, when stacked together and placed close to a target, provide a simple method of imaging a laser-generated proton beam with a high degree of spatial and spectral resolution (depending on the stack composition).

With the development of new ultra-high intensity, high repetition rate facilities, such as Astra Gemini, new diagnostics are required that are capable of acquiring data on a shot-to-shot basis. RCF stacks, while providing a well-calibrated method of characterising a proton beam, are time-consuming to construct and can only be used for a single shot before having to be replaced. Here we present a new diagnostic that has been designed to address these issues by using plastic scintillators as an imaging medium. The fundamental design of the diagnostic is outlined together with the first results that have been obtained on a recent Astra Gemini experiment.

## Instrument layout

The proton footprint monitor works by collecting light that is emitted from a plastic scintillator when protons are stopped within the material. The scintillated light is relayed via a number of mirrors and is recorded using a CCD camera, providing a near-instant image of the proton beam profile without the need for the removal and scanning of RCF.

Each scintillator replicates a single layer of a conventional passive stack, hence multiple scintillators are required to achieve a profile of the beam energy spectrum. The thickness of each scintillator determines the energy resolution, with five or more scintillators typically being required for a suitably wide energy range.

In order to maximise the number of proton energy bins in the diagnostic scintillators were arranged in pairs, each with a different central emission wavelength. By doing this, one set of optics and one camera could be used to image two beam profiles at a time. The two signals are separated by mounting a prism beam splitter together with two interference filters on the front of the camera lens; each filter wavelength centred close to that of one scintillator.

The light emitted from each pair of scintillators is relayed to a separate gated CCD camera. Gated CCD cameras were used to isolate the proton signal from both stray laser light and any scintillated light that could result from additional ionising radiation; e.g. fast electrons or X-rays, both of which can be produced in significant numbers normal to the target rear surface during the laser-plasma interaction.

By choosing scintillators with a fast (~ns) response time (characterized by the rise and fall time for light emission), the light signal generated by the lower velocity protons can be clearly separated from any preceding high velocity electrons and X-rays.

In designing the diagnostic, the distance from the target to the scintillators was chosen so that the temporal separation between protons and other ionising radiation was greater than both the response time of the scintillator and the gating time of the CCD camera. The CCD cameras used for the diagnostic, 16-bit Princeton Instruments PI-Max 1024, have a minimum gating time as short as 0.5 ns, hence the spacing requirement of the scintillators was largely determined by their response time. Two

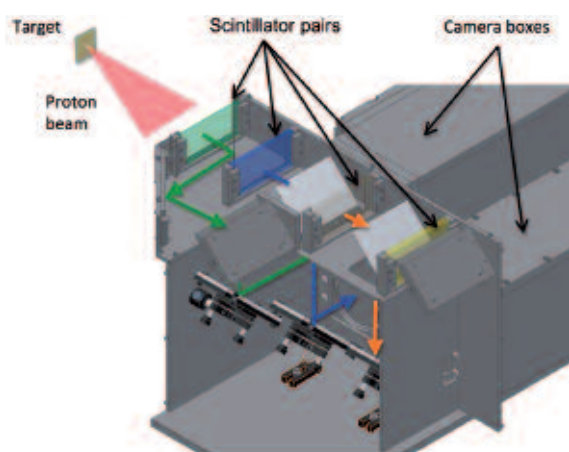


**Figure 1. Internal layout of the footprint monitor. The diagnostic is capable of holding four pairs of scintillators. The light output from each pair (coloured arrows) is routed to a separate gated camera.**

types of polyvinyltolouene scintillators were used, both of which were manufactured by Saint Gobain. The first (BC-422Q) has the fastest response time of 0.7 ns and a central emission wavelength of 370 nm. The second (BC-408) is slower at 2.1 ns with a wavelength of 425 nm.

The scintillators and subsequent optics are all contained within a light tight box which is kept under vacuum during shots. The gated cameras are housed in separate vessels (kept at air for operation of the cameras) which were connected to the main box via 120 mm glass windows. An aluminium coated 200  $\mu\text{m}$  fused silica pellicle was attached to the front of the diagnostic to prevent laser light from entering the diagnostic and to protect the first pair of scintillators from debris.

The scintillator configuration was chosen by taking into consideration what proton energy range was required for observation. SRIM (Stopping Range of Ions in Matter)<sup>[6]</sup> was used to calculate what proton energies would be stopped at each layer of material (see Table 1). Only the first two scintillator layers are shown corresponding to the data presented in this report.

The spatial resolution of the diagnostic is determined jointly by the scintillator material and the subsequent imaging optics and CCD camera system. Measurements offline of the first scintillator pair found a spatial resolution of 1 mm over a visible area of 78 $\times$ 63 mm.

Layer composition absorbed	Thickness	Proton energies
Fused silica pellicle	200 $\mu\text{m}$	< 5 MeV
BC-408	400 $\mu\text{m}$	5-8 MeV
BC-422Q	400 $\mu\text{m}$	8-10 MeV

**Table 1. Proton energies absorbed in the first few layers of the footprint monitor.**

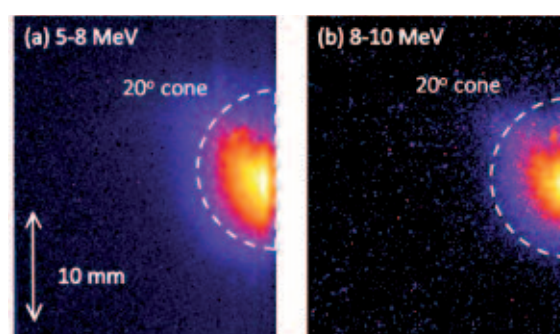


**Figure 2. Proton footprints for two energy windows for a 100 nm Al target shot at high contrast ( $> 10^9$ ) at an intensity of  $\sim 5 \times 10^{20} \text{ Wcm}^{-2}$ .**

### Experimental setup

The experiment was performed on the Astra Gemini laser facility at the Rutherford Appleton Laboratory. A single ultra-intense short pulse beam was used to irradiate a broad range of thin foil targets; from 20  $\mu\text{m}$  Aluminium to 10 nm Carbon. The targets were orientated at an angle of 35° relative to the laser incident direction. Approximately 10 J of energy was focused on target using an F/2 off-axis parabola with a pulse duration of 50 fs, giving a focused intensity of up to  $1 \times 10^{21} \text{ Wcm}^{-2}$ . The first data set was obtained without any laser contrast enhancement ( $\sim 10^7$  contrast). The second data set was collected using a double plasma mirror setup<sup>[7]</sup>; increasing the laser contrast to at least  $10^9$ . This contrast enhancement enabled the shooting of ultra-thin ( $< 50 \text{ nm}$ ) foils without any significant pre-pulse disturbance.

The footprint diagnostic was positioned in the Astra Gemini chamber normal to the target rear surface such that the first scintillator was approximately 12 cm from the interaction point. An array of Thomson parabolas were also directed at the rear surface of the target to obtain proton and ion spectra. As a result the footprint monitor was positioned below the target interaction horizontal in order to sample the lower half of the proton beam only. For the purpose of data analysis a certain degree of beam symmetry has to be assumed.

### Initial results

During commissioning of the diagnostic on the experiment only two pairs of scintillators were used, together with two of the gated cameras. However, limited proton fluxes at higher energies obtained during the experiment ( $> 10 \text{ MeV}$ ) meant that only the first two scintillators were able to provide images of the proton beam. We present these data below.

Figure 2 shows two images of a proton beam obtained for two energy windows (5-8 MeV and 8-10 MeV) for a 100 nm Al target irradiated at best focus ( $\sim 5 \times 10^{20} \text{ Wcm}^{-2}$ ) with high contrast ( $> 10^9$ ) laser pulses. The similar beam profiles and divergences (8° and 10° respectively for figure 2a and 2b) would be expected with such close energy bands. It is necessary to go to higher proton energies in order to have broader separation between the scintillator energy windows, yielding distinctive energy dependent changes in the beam footprint.

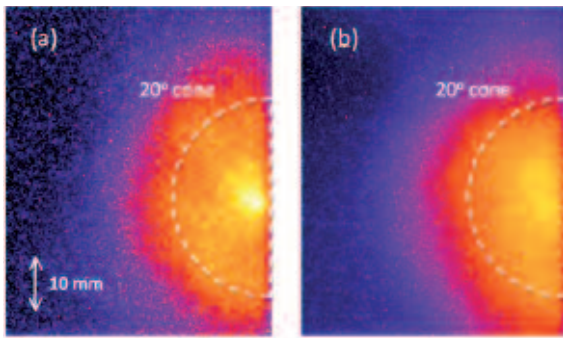


**Figure 3.** Proton footprints showing the lower half of the proton beam in the energy range of 5-8 MeV obtained with a low contrast ( $\sim 10^7$ ) beam, focused to an intensity of  $\sim 1 \times 10^{21} \text{ Wcm}^{-2}$  onto a) 20  $\mu\text{m}$  Au and b) 20  $\mu\text{m}$  Al targets. The 20° half-cone is shown for reference.

While qualitative observations of ccd counts provides an indication of proton flux, quantitative measurements require calibration of the scintillator and associated optics. This is expected to be performed over the coming months with access to a characterised cyclotron proton source.

Typical measurements made without any laser contrast enhancements are shown in figure 3. Proton beams obtained at an intensity of  $1 \times 10^{21} \text{ Wcm}^{-2}$  are shown for both 20  $\mu\text{m}$  Au and Al targets. Both beams have a similar profile in the 5-8 MeV range, with full cone angles of 20° and 24° respectively.

With plasma mirrors in place a large number of high contrast shots were taken using a range of thin (10 nm – 6  $\mu\text{m}$ ) Al and C targets. A significant reduction in beam divergence was observed over all target thicknesses and materials under high contrast conditions. However beam pointing and shape were seen to vary from shot to shot. Two typical proton beams are shown in figure 4 for similar thin Al targets.

The physics behind the marked reduction in beam divergence with increasing laser contrast is currently the subject of further investigation. With the switch to high contrast conditions it is possible that any pre-heating of the target rear surface due to ns-scale pre-pulse would have been minimised, thus reducing rear surface distortion and hence the spread in proton emission angles<sup>[18]</sup>. However, since the divergence angles observed were largely independent of target thickness (for 3-20  $\mu\text{m}$  Al) at low contrast, it is possible that another effect is responsible for the change in beam divergence with contrast. Possible changes in laser absorption and subsequent fast electron transport with laser contrast will be examined as part of the investigation.

The beam positioning on the footprint monitor has particular relevance when analysing the results from the Thomson parabolas. For some shots (figure 4(a)) the bulk of the proton beam was seen to be positioned almost entirely on the scintillator. The corresponding Thomson spectra for the same shot was noticeably weak as a result. Hence by noting the beam size and position, the footprint monitor can be used to distinguish between shots that exhibit a weak Thomson spectra due to poor shot conditions, thus allowing for an immediate repeat of that shot, and

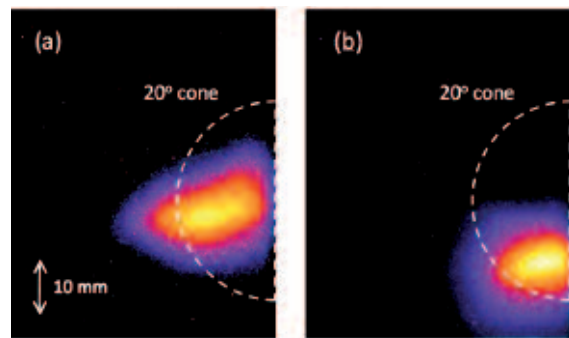


**Figure 4.** Proton footprints showing the lower half of the proton beam in the energy range of 5-8 MeV obtained with a high contrast ( $> 10^9$ ) laser pulse with an intensity of  $\sim 5 \times 10^{20} \text{ Wcm}^{-2}$  onto a) 800 nm Al and b) 500 nm Al targets.

those which produce a strong proton beam but with an unusual pointing.

### Conclusions and future development

An in-situ scintillator diagnostic for imaging laser-produced proton beams has been designed and commissioned in Astra Gemini for the first time. The diagnostic was used to obtain measurements of proton beam divergence and pointing under high and low laser contrast conditions. While the initial fielding of the footprint monitor on the Astra Gemini experiment was successful, several key points need to be addressed if the diagnostic is going to be used as a direct replacement for conventional, passive detection methods.

Firstly the extensive calibration of the scintillators must be performed in order that quantitative measurements of proton flux can be obtained. This needs to be done over a wide range of controlled proton energies to enable the diagnostic to be used with a flexible configuration of energy windows.

Secondly the light flux collected from each scintillator has to be maximised in order to obtain a sufficient signal to noise ratio and a high level of spatial resolution. A future design of the diagnostic will aim to replace the scintillator-camera optical path with a fibre optic channel that will minimise both light loss and the amount of space taken up inside the interaction chamber by the diagnostic.

### Acknowledgements

The authors gratefully acknowledge the assistance of the Central Laser Facility staff at the Rutherford Appleton Laboratory. The work has been supported as part of the LIBRA EPSRC grant EP/E035728/1.

### References

1. E. L. Clark *et al.*, *Phys. Rev. Lett.* **84**, 670 (2000).
2. R. A. Snavely *et al.*, *Phys. Rev. Lett.* **85**, 2945 (2000).
3. A. J. Mackinnon *et al.*, *Phys. Rev. Lett.* **86**, 1769 (2001).
4. S. C. Wilks *et al.*, *Phys Plasmas* **8**, 542 (2001).
5. P. Mora *et al.*, *Phys. Rev. Lett.* **90**, 185002 (2003).
6. L. O. Silva *et al.*, *Phys. Rev. Lett.* **92**, 15002 (2004).
7. T. Esirkepov *et al.*, *Phys. Rev. Lett.* **92**, 175003 (2004).

8. A. P. L. Robinson *et al.*, *Phys. Rev. Lett.* **96**, 035005 (2006)
9. P. K. Patel *et al.*, *Phys. Rev. Lett.* **91**, 125004 (2003)
10. R. A. Snavely *et al.*, *Phys. Plasmas* **14**, 092703 (2007).
11. D. C. Carroll *et al.*, *Phys. Rev. E* **76**, 065401 (2007).
12. M. Roth *et al.*, *Phys. Rev. Lett.* **86**, 436 (2001).
13. S. Atzeni *et al.*, *Nuclear Fusion* **42**, L1 (2002).
14. S. V. Bulanov *et al.*, *Physics Letters A* **299**, 240 (2002).
15. N. V. Klassen *et al.*, *Medical Physics* **24**, 1924 (1997).
16. J. F. Ziegler <http://www.srim.org/> (2008).
17. B. Dromey *et al.*, *Rev. Sci. Instrum.* **75**, 645 (2004).
18. F. Lindau *et al.*, *Phys. Rev. Lett.* **95**, 175002 (2005).